Supplementary Materials

Title: HER3-Mediated Resistance to Hsp90 Inhibition Detected in Breast Cancer Xenografts by Affibody-based PET Imaging

Authors: Carlos D. Martins[1], Chiara Da Pieve[1], Thomas A. Burley[1], Rhodri Smith[1], Daniela M. Ciobota[1], Louis Allott[1], Kevin J. Harrington[1], Wim J.G. Oyen[1, 2], Graham Smith[1], Gabriela Kramer-Marek[1*]

Affiliations:
[1]Division of Radiotherapy and Imaging, The Institute of Cancer Research, 123 Old Brompton Road, London, SW7 3RP, UK
[2]The Royal Marsden NHS Foundation Trust, Department of Nuclear Medicine, Fulham Road, London, SW3 6JJ, UK

Contents:

Materials and Methods

Cell lines

The genetic origin of cell lines was authenticated by short tandem repeat (STR) DNA profiling analysis (Eurofins Medigenomix, Germany). Results were compared with STR profiles published online at https://www.dsmz.de/services/services-human-and-animal-cell-lines/online-str-analysis.html, matching for the following markers: amelogenin, CSF1PO, D16S539, D5S818, D7S820, TH01, TPOX, D13S317 and vWA. All the cells were routinely tested and found to be negative for Mycoplasma contamination (PCR detection kit, Surrey Diagnostics Ltd, Cranleigh, UK).

Preparation of the DFO-$Z_{HER3:8698}$ conjugate

The conjugation of deferoxamine-maleimide (DFO-mal, Macrocyclics, USA) to the $Z_{HER3:8698}$-Cys affibody molecules (AffibodyAB, Sweden) was performed as previously described (1). Briefly, in a 1.5 mL low ultra-high recovery microcentrifuge tube (Starlab Group, UK), a solution of $Z_{HER3:8698}$-Cys (300 µL, 1.6 mg/mL in PBS, 68.4 nmol) was diluted with PBS (130 µL, Gibco, UK)) and 0.1 M ethylenediaminetetraacetic acid (EDTA, Sigma-Aldrich, UK) solution (60 µL). Subsequently, freshly prepared tris-(2-carboxyethyl)-phosphine hydrochloride (TCEP-HCl, Thermo Scientific, UK) (9.8 µL, 0.05 mg/µL in PBS, 1.71 µmol) was added and the mixture was incubated in a thermomixer at 85°C for 5 min (800 rpm) followed by 25 min at room temperature (RT). Then DFO-mal (2.0 mg, 2.8 µmol) in dimethyl sulfoxide (DMSO, Fisher Scientific, UK) (50 µL) was added and the solution was incubated in a thermomixer at 40°C for 2 h (800 rpm). The reaction mixture was analyzed by analytical reverse-phase HPLC (RP-HPLC) using gradient 1 (Supporting Information). The product was purified by semi-preparative RP-HPLC. The collected fractions containing the product were lyophilized using a concentrator plus (Eppendorf, UK) and quantified by measuring the UV absorbance at 280 nm on a NanoDrop 2000 spectrophotometer using the coefficient of 0.428 mg/mL (Thermo Scientific, UK) to yield 254 µg of DFO-$Z_{HER3:8698}$ (48.1% yield). Analytical RP-HPLC: R_t = 9:04 (min:sec) MALDI-MS (*m/z*): $[M + H]^+$ expected: 7720, found: 7720.6.

Preparation of the DFO-Z_{TAQ} conjugate

Z_{TAQ}-Cys affibody is a Z_{TAQ}-polymerase binding affibody that was used as a negative control. TAQ polymerase does not naturally occur in cells so Z_{TAQ} is not supposed to bind to or affect the cells. In a 1.5 mL low protein binding centrifuge tube, a solution of Z_{TAQ}-Cys (100 µL, 2.0 mg/mL in PBS, 29.3 nmol. Affibody, Sweden) was diluted with PBS (50 µL) and 0.1 M EDTA solution (26 µL). A freshly prepared solution of TCEP-HCl (4.0 µL, 0.05 mg/µL in PBS, 0.73 µmol) was added and the mixture was incubated in a thermomixer at 85°C for 5 min (800 rpm) followed by 25 min at RT. DFO-mal (0.75 mg, 1.0 µmol) in DMSO (30 µL) was then added and the solution was incubated in a thermomixer at 40°C for 2 h (800 rpm). The reaction mixture was analyzed by analytical RP-HPLC using gradient 2 (Supporting Information). The product was purified by semi-preparative RP-HPLC. The collected fractions containing the product were lyophilized and quantified by measuring the UV absorbance at 280 nm on a Nanodrop 2000 spectrophotometer using the coefficient of 0.619 mg/mL (61.5 µg, 28% yield). Analytical RP-HPLC: R_t = 10:19 (min:sec) MALDI-MS (*m/z*): $[M + H]^+$ expected: 7520, found: 7520.6.

Preparation of ^{89}Zr-labeled DFO- affibody conjugates

Radiolabeling was performed following a published procedure (2). To optimize the radiolabeling efficiency (>95%), several small reactions (containing max 18 MBq of ^{89}Zr-oxalic acid solution) were performed in preference of a large single reaction. Briefly, the required amount of ^{89}Zr-oxalic acid solution (16-17.5 MBq, Cyclotron, NL) was transferred into a 1.5 mL low protein binding centrifuge tube followed by a freshly prepared 2.0 M sodium carbonate solution (Na_2CO_3, Sigma-Aldrich, UK) in a 1:0.64 (v/v) ratio. The mixture was incubated for 3 min at RT. Successively, 0.5 M HEPES (pH 7.1, Sigma-Aldrich, UK) was added to the solution in a 2.3:1 HEPES to ^{89}Zr-oxalic acid solution (v/v) ratio (0.32 M final concentration) followed by DFO-conjugate solution (1 mg/mL, 6.4-7.0 µL) in HEPES pH 7.1. The mixture was incubated for 1 h at RT. The radiolabeling efficiency was determined by ITLC using ITLC-SG strips and 0.1 M citrate buffer (pH 5.0) as eluent. The ^{89}Zr-labeled DFO-conjugate appeared at the origin (R_f = 0.0-0.1) while the $^{89}Zr^{4+}$, which was not bound to the affibody molecules, run with the solvent front (R_f = 0.9-1.0).

In vitro serum stability assay of ^{89}Zr-DFO-$Z_{HER3:8698}$

The stability of ^{89}Zr-DFO-$Z_{HER3:8698}$ with respect to loss of radioactivity from the radiolabeled affibody molecules was assessed by incubating the radioconjugate (~2 MBq) in mouse serum (500 µL, Sigma-Aldrich, UK) in a thermomixer at 37°C (300 rpm). Samples were taken at 0, 3 and 24 h and analyzed by ITLC-SG. ^{89}Zr-oxalate solution (~2 MBq) incubated in mouse serum (500 µL) was processed in the same way and used as a control.

^{89}Zr-DFO-$Z_{HER3:8698}$ *in vitro* binding affinity and specificity

The dissociation constant (K_d) of ^{89}Zr-DFO-$Z_{HER3:8698}$ was assessed by a saturation binding assay using HER3 highly-expressing MCF-7 cells. The cells (6.5×10^5) were seeded on 12-well plates and cultured overnight. After removing the growth medium, the cells were washed with PBS and incubated with increasing concentrations of the radioconjugate (final concentrations of 0.01, 0.1, 0.25, 0.5, 1.0, 1.5, 2.0 and 3.5 nM, 0.12-47 kBq/well) diluted in non-supplemented DMEM (1 mL). Non-specific binding was determined by pre-incubating the cells with 100-fold molar excess of the non-radiolabeled affibody molecules for 10 min. After 1 h incubation at 4°C, the cells were rinsed twice with cold PBS prior to detachment with trypsin-EDTA (1x) (Gibco, Life technologies, UK). Subsequently, the cells were collected into scintillation vials (PerkinElmer, UK) and the total cell-associated radioactivity was measured using a 2480 WIZARD^2 Automatic Gamma Counter (PerkinElmer, UK). To estimate the K_d, the data were plotted as the amount of bound (nM) *vs.* free radioconjugate (nM). The specific binding was determined by subtracting the fraction of non-specific binding from the total binding, and fitted to a one-site receptor-binding model using GraphPad Prism v7.0. The specificity of binding of the radioconjugate was evaluated using MCF-7, BT-474, MDA-MB-468 and MDA-MB-231 cells (6.5×10^5) plated on 12-well plates, 24 h prior to the study. The cells were pre-incubated with a 100-fold molar excess of either the non-radiolabeled affibody molecules or the natural ligand heregulin (HRG), (R&D Systems, UK), for 10 min at 4°C, followed by incubation with ^{89}Zr-DFO-$Z_{HER3:8698}$ (1 nM, ~11.93 kBq/well) for 1 h at 4°C. Afterwards, cells were rinsed twice with cold PBS, trypsinized, and collected into scintillation vials. The radioactivity was assessed using a gamma counter. The specificity of binding was normalized to the maximum cell-associated radioactivity per experiment and presented as the mean of $n = 3$ independent measurements ± SEM.

Immunohistochemistry

Formalin-fixed tumors (10%, v/v) were embedded in paraffin, sectioned into 3 μm-thick slices, and mounted on microscope slides. Multiple sections were taken at regular intervals across each tumor, with sequential sections being stained with H&E (Leica, Germany), anti-CD31 mAb (1:75, DIA310, Dianova, Germany) and anti-HER3 mAb (1:50, M7297, Dako, UK). Sections to be stained against CD31 were pre-treated in a pressure cooker for 2 min in buffer solution pH 9.0 (H3301, Vector Labs, UK), followed by endogenous peroxidase blocking (S2023, Dako, UK) for 5 min at RT. Incubation with the primary antibody was performed for 1 h at RT, followed by detection for 30 min at RT using Rat Histofine MaxPO (414311F, 2B Scientific, UK). For HER3 staining, heat-mediated antigen retrieval was conducted at 97°C for 40 min, with Dako retrieval buffer, pH 9.0. HER3 staining was performed for 1 h at RT, followed by detection using the Envision FLEX+ for Mouse kit (K800221, Dako, UK) according to the manufacturer protocol.

Immunoblotting analysis

Rabbit monoclonal antibodies against HER2 (1:1000), EGFR (1:1000), IGF-1Rβ (1:500), c-MET (1:500), MAPK (1:1000), phospho-HER3-Y1289 (1:500), phospho-HER2-Y1248 (1:500), phospho-EGFR-Y1068 (1:500), HRG (1:250), PI3K (1:500), phospho-AKT-S473 (1:500), GAPDH (1:1000), and mouse monoclonal antibodies against N-Cadherin (1:500) and phospho-MAPK-T202/Y204 (1:500) were purchased from Cell Signaling Technology, UK. Mouse monoclonal antibodies against HER3 (1:400) and Hsp70/72 (1:2500) were obtained from Merck Millipore, UK and Enzo Life Sciences, UK, respectively. The blots were incubated overnight at 4^{o}C with the indicated primary antibodies, followed by horseradish peroxidase-conjugated secondary antibody incubation and subsequent detection by enhanced chemiluminescence reagent (Pierce, UK). Finally, the membranes were scanned using a ChemiDoc™ XRS+ System (Bio-Rad, UK). Densitometric analysis was performed using ImageQuant TL Version 8.1 (GE Healthcare Life Sciences, UK). Data are represented as the mean ± SEM ($n = 2$ independent experiments).

Proliferation assay

MCF-7 and BT-474 cells were plated on 96-well plates at cell densities of 1.8×10^4 and 6×10^3 cells/well, respectively, and allowed to attach for 24 h. Subsequently, media were aspirated and the cells were incubated with 32 nM of AUY922, and/or 10 μM of PPP for 72 h. Control cells were incubated with the highest DMSO-equivalent concentration. The plates were inserted into an Incucyte Zoom imaging system (Essen BioScience, USA) at 37°C and 5% CO_2 humidified air. Each well was imaged by phase contrast every 2 h for 72 h. Afterwards, images were collected and the percentage (%) of confluence, which indicates the % of the image occupied by cells, was determined using software provided by the manufacturer. The % confluence was averaged over 4 fields of view per well, across the wells receiving the same treatment. The data were plotted as the normalized confluence to control over time.

Scratch-wound assay

MCF-7 and BT-474 cells were plated to 100% confluence on 96-well plates (Essen BioScience, USA) at cell densities of 3×10^4 and 7.5×10^4 cells/well, respectively, and allowed to attach for 24 h. The wound was inserted in the center of each well using a Woundmaker (Essen BioScience, USA). Subsequently, the media

were aspirated and the cells were exposed to 32 nM of AUY922, and/or 10 μM of PPP for up to 72 h. Control cells were incubated with the highest DMSO-equivalent concentration. The plates were placed in an Incucyte Zoom imaging system at 37°C and 5% CO_2 humidified air. The wound on each well was imaged by phase contrast every 2 h for a total period of 72 h. The images were collected and processed using the software provided by the manufacturer. The invasiveness/motility per time point was indicated as the relative wound density (RWD), which is the spatial cell density in the wound area relative to the spatial cell density outside the wound area. The RWD is 0% when the wound is inserted (at time zero) and 100% when the spatial cell density in the wound area is the same as the density outside this area, making it a self-normalizing metric. The RWD was averaged across the wells receiving the same treatment.

Animal studies

Mice receiving MCF-7 or BT-474 cells were implanted with 17β-estradiol pellets (0.72 mg/90 or 0.36 mg/90 days release, respectively, Innovative Research of America, USA) 48 h before cell inoculation. The pellets remained in place until the end of the study. Tumors were allowed to grow for 2-4 weeks until reaching the volume of approximately 100 mm^3 before being used for imaging studies. AUY922 treatment studies were conducted using MCF-7 and BT-474 xenografts. MCF-7 tumor bearing mice received 8 doses of AUY922 (40 mg/kg) and BT-474 6 doses (50 mg/kg) delivered via intraperitoneal (i.p.) injection, over the course of 2 weeks. Mice were randomized into either treatment (n = 4-7) or control (n = 4-6) groups, and subsequently injected with ^{89}Zr-DFO-$Z_{HER3:8698}$. PET/CT images were acquired before treatment initiation and/or following administration of the last AUY922 dose. Mouse weight was monitored at the time of treatment, with no discernible loss observed in the treatment group.

PET imaging studies

The mice were anesthetized using an isoflurane/O_2 mixture (1.5-2.0 % v/v) ~ 5 min prior to imaging. After administration of the radioconjugate (3 μg in 100 μL of sterile 0.9% sodium chloride solution, 7.2-8.1 MBq/mouse) by intravenous tail vein injection (i.v.), the mice were placed prone in the center of the scanner's field of view. Whole body PET static images were acquired 3 h post radioconjugate injection for the duration of 15 min with a 358 to 664 keV energy window, followed by CT acquisition. The imaging data were normalized to correct for PET non-uniformity, dead-time count losses, positron branching ratio, and physical decay to the time of injection. No attenuation or partial-volume averaging corrections were applied. The PET images were reconstructed using a MLEM algorithm (12 iterations) with a voxel size of 0.5 × 0.5 × 0.5 mm^3. Whole body standard high resolution CT scans were performed with the X-ray tube set-up at a voltage of 45 kV, current of 400 μA, 250 projections (1 sec per projection) and a voxel size of 0.5 × 0.5 × 0.5 mm^3. The CT images were reconstructed using a filtered back projection (FBP) algorithm. Image analysis was performed using the PMOD software package (PMOD Technologies Ltd, CH). Tumor segmentation was performed using a 50% threshold. The mean counts (PET Mean) and the PET Peak (mean of the 500 voxels with highest counts within the tumor volume) were recorded per mouse and converted into percentage of the injected dose per gram of tissue (%ID/g) by means of a calibration factor (MBq/g/counts) determined from scanning a ^{89}Zr source of known activity and volume.

Texture Analysis

The tumors were segmented from the ^{89}Zr-DFO-$Z_{HER3:8698}$ images obtained on days 0 and 14 for both control and treated mice. First, second and higher order texture parameters were extracted as previously described *(3)*, with second order statistics collected in x, y and z directions. A total of 89 parameters were extracted. Moreover, two instances of the LDA model were built, first using the %ID/g parameter, and second with all the 89 extracted texture features. A leave-one-out cross-validation was performed, whereby, on each iteration one mouse was left out of the model construction and used as a "test" mouse, resulting in 13 different instances of both models. The LDA models were assessed by examining their ability in successfully classifying the test mouse, as treated or control.

Tumor *ex vivo* autoradiography

Tumors were dissected and immediately embedded in an optimal-cutting-temperature compound (Tissue-Tek, USA), and frozen on dry ice. Subsequently, the frozen tissue was sectioned into 6 μm-thick slices using a cytomicrotome (Thermo Fisher Scientific, UK), mounted on slides and left to air-dry. The sections were imaged using the phosphor technology module of a Typhoon FLA7000 scanner (GE Healthcare Life Sciences, UK).

Statistical analyses

Statistical significance was determined using unpaired two-tailed Student's t tests with Welch's correction. Three mice per model were allocated for *in vivo* assessment of ^{89}Zr-DFO-$Z_{HER3:8698}$ specificity. Sample size was calculated with a power of 90% and a significance level of 5% based on the effect determined by the difference in cell-associated radioactivity between MCF-7 and MDA-MB-231 cells. Six to seven MCF-7

xenografts per group were used for the *in vivo* evaluation of AUY922 treatment response using ^{89}Zr-DFO-$Z_{HER3:8698}$ imaging. The sample size was calculated with 90% power and 5% significance level. The mice were randomized before treatment initiation. No data were excluded from the analysis, including all outliers. Three experimental replicates were performed for the *in vitro* data. For the analysis of ^{89}Zr-DFO-$Z_{HER3:8698}$ uptake in multiple xenograft models, significance was determined by analysis of variance (ANOVA) with Tukey's honest significance test for correction of multiple comparisons. Correlation analysis was performed using Spearman's rank correlation, with linear regression, 95% confidence intervals, and statistical significance determined using Prism software (GraphPad Software v7.0). Statistically significant differences between groups were assumed if $P \leq 0.05$.

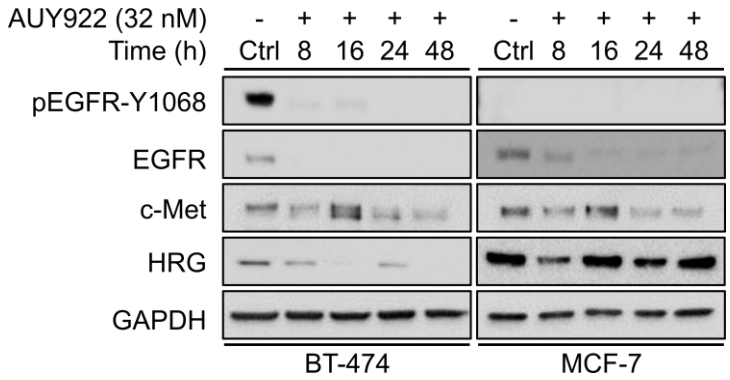

Fig. S1. Time course of AUY922 treatment in BT-474 and MCF-7 cells. Treatment with the Hsp90 inhibitor AUY922 (32 nM) was carried out up to 48 h. Total and phosphorylated EGFR receptor, c-Met, and HRG protein levels were monitored by WB using whole cell lysates. GAPDH was used as a loading control.

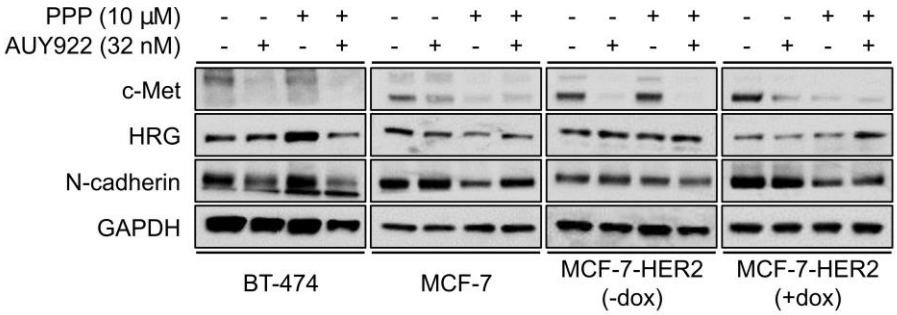

Fig. S2. Effects of AUY922 and PPP treatment in low and high HER2-expressing breast cancer cell lines. BT-474 (high HER2), MCF-7 (low HER2), MCF-7-HER2 (-dox, induced HER2 expression), and MCF-7-HER2 (+dox, non-induced HER2) cells were treated with AUY922 (32 nM) and/or PPP (10 μM) for 48 h. c-Met, HRG, and N-cadherin protein levels were monitored by WB using whole cell lysates. GAPDH was used as a loading control.

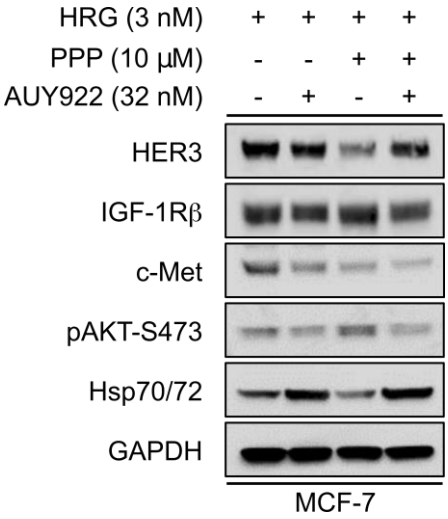

Fig. S3. Effect of HRG stimulation in AUY922 and PPP treated MCF-7 cells. MCF-7 cells were treated with AUY922 (32 nM) and/or PPP (10 μM) for 48 h, followed by stimulation with 3 nM of HRG at 37°C for 10 min before cell lysis. HER3 receptor, IGF-1Rβ, c-Met, and PI3K/AKT pathway activation were monitored by WB using whole cell lysates. Hsp70/72 expression was used as a surrogate for AUY922 treatment efficacy, and GAPDH as a loading control.

	HER3			IGF-1Rβ		
Cell line	**AUY922**	**PPP**	**AUY922 + PPP**	**AUY922**	**PPP**	**AUY922 + PPP**
BT-474	0.60 ± 0.17	0.59 ± 0.10	0.28 ± 0.24	0.9 ± 0.26	0.37 ± 0.11	0.40 ± 0.17
MCF-7	0.95 ± 0.03	0.36 ± 0.12	0.63 ± 0.30	0.96 ± 0.09	1.01 ± 0.29	0.88 ± 0.17
MCF-7 HER2+++	0.67 ± 0.08	0.97 ± 0.08	0.66 ± 0.05	0.76 ± 0.06	0.99 ± 0.06	0.54 ± 0.01
MCF-7 HER2 +	0.75 ± 0.18	0.76 ± 0.03	0.72 ± 0.06	0.70 ± 0.06	0.69 ± 0.14	0.49 ± 0.08

Table S1. Densitometric analysis of Western blots pertaining to the treatment of BT-474, MCF-7, MCF-7 HER2+++ (-dox), and MCF-7 HER2+ (+dox) following 48 h treatment with AUY922 and PPP alone, or in combination. All cell lines were treated with AUY922 (32 nM) and/or PPP (10 μM) for 48 h before cell lysis. HER3 receptor and IGF-1Rβ, c-Met, and PI3K/AKT pathway activation were monitored by WB using whole cell lysates. Hsp70/72 expression was used as a surrogate for AUY922 treatment efficacy, and GAPDH as a loading control. Densitometric analysis was performed for the HER3 receptor and IGF-1Rβ, relative to the loading control. Expression levels were normalized to each control sample per cell line. Data are represented as mean ± SEM (*n* = 2 independent experiments).

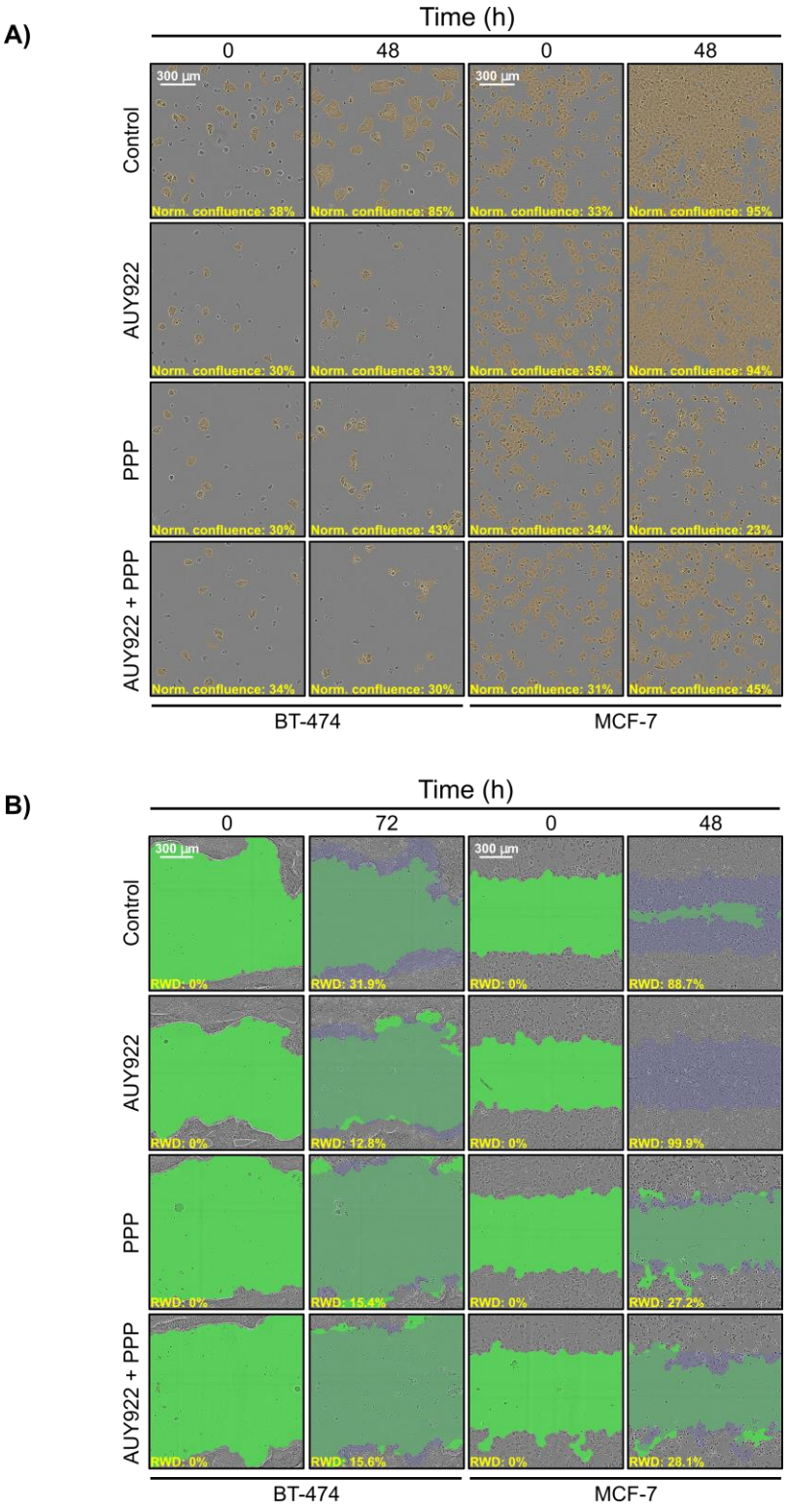

Fig. S4. AUY922 and PPP treatment effect on the proliferative and invasive phenotype of BT-474 and MCF-7 breast cancer cells. BT-474 and MCF-7 cells were treated with AUY922 (32 nM) and/or PPP (10 µM) up to 72 h. **(A)** Representative micrographs of the proliferation data presented in Fig. 3C and D. The orange mask illustrates the individual objects detected and used to calculate confluence per time point. The normalized to control confluences are indicated in each image. **(B)** Representative micrographs of the scratch-wound data presented in Fig. 3E and F. The green mask represents the wound region that is not populated. The blue mask illustrates the portion of the original wound region, which has become populated with cells. The relative wound density (RWD) percentages are indicated per image.

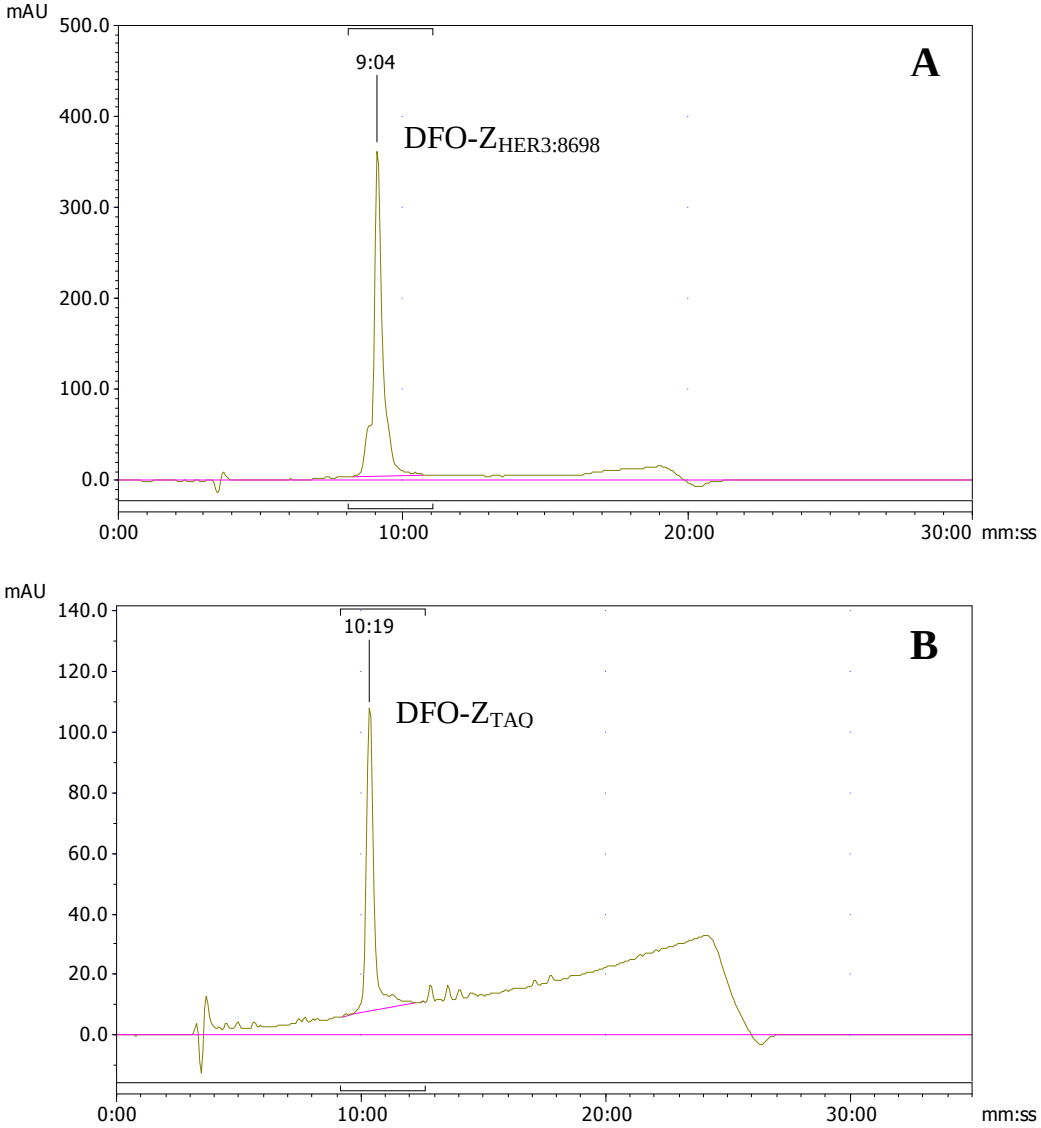

Fig. S5. **HPLC chromatograms of purified DFO-affibody conjugates.** (**A**) DFO-$Z_{HER3:8698}$ and DFO-Z_{TAQ} (**B**) chromatograms were obtained using gradients 1 and 2, respectively. The absorbance was recorded at a 230 nm wavelength. Analytical and semi-preparative HPLC were carried out on an Agilent Infinity 1260 quaternary pump system equipped with a 1260 Diode array (Agilent Technologies). Elution profiles were analyzed using Laura software (Lablogic, Sheffield, UK). Affibody conjugates were analyzed on a Zorbax-300SB-C18 column, 7.8 × 250 mm, 5 µm (Agilent Technologies) using either Gradient 1: 0-12 min. 23%-35% B, 12.1-15 min. 35%-50% B; 15.1-16 min. 50%-23% B or Gradient 2: 0-20 min. 30%-65% B, 20.1-22 min. 65%-30% B with 0.1% TFA in water as eluent A and 0.1% TFA in acetonitrile as eluent B at a flow rate of 1 mL/min. Affibody conjugates were purified by semi-preparative RP-HPLC on a Jupiter C18 column, 10 × 250 mm, 10 µm, 300 Å (Phenomenex), using either Gradient 1 or 2 at a 3 mL/min flow rate. HPLC grade acetonitrile and trifluoroacetic acid (TFA) were purchased from Fisher Scientific (Loughborough, UK).

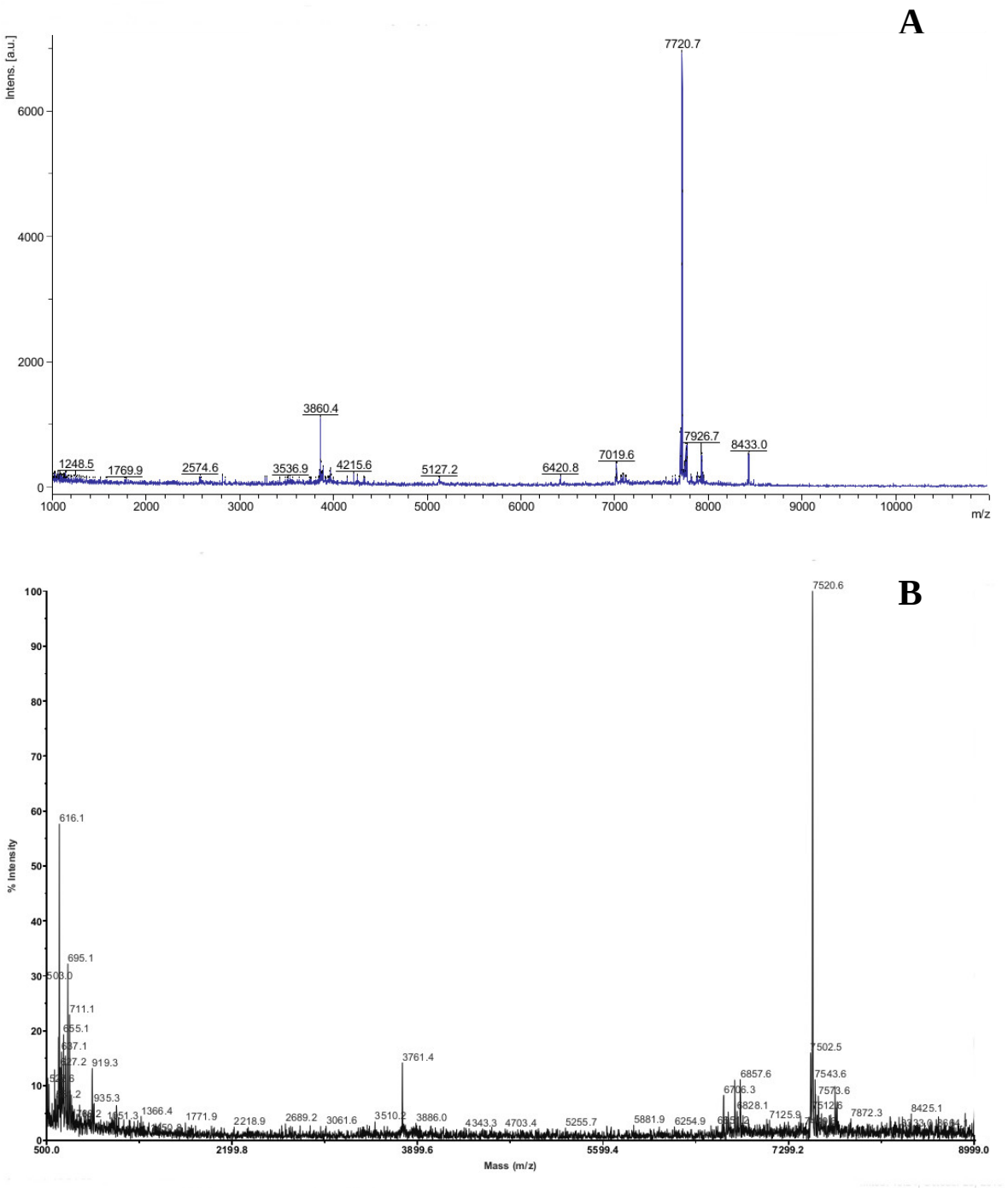

Fig. S6. **MALDI-MS spectra of purified DFO-$Z_{HER3:8698}$ (A) and DFO-Z_{TAQ} (B).** Matrix-assisted laser desorption ionization mass spectrometry (MALDI-MS) analyses were performed by the EPSRC UK National Mass Spectrometry facility at Swansea University, UK. A. MALDI-MS (*m/z*): $[M + H]^+$ expected: 7720, found: 7720.6; B. MALDI-MS (*m/z*): $[M + H]^+$ expected: 7520, found: 7520.6.

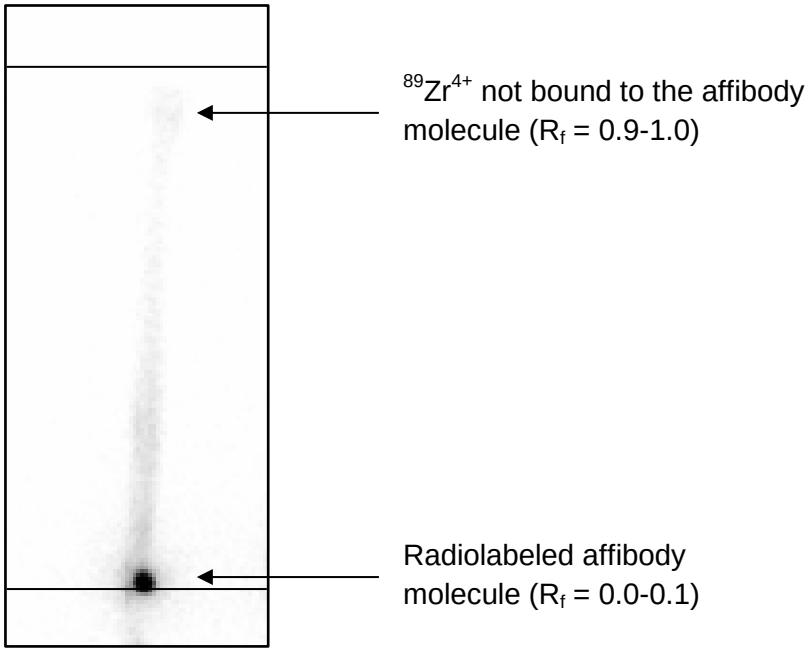

Fig. S7. Representative radio-ITLC of the crude radiolabeling mixture of ^{89}Zr-DFO-$Z_{HER3:8698}$. Radio-ITLC was run on silica-impregnated ITLC strips using 0.1 M citrate buffer (pH 5.0) as the mobile phase. The radiolabeled protein remains at the origin (R_f = 0.0-0.1) while un-bound radiometal migrates with the solvent front (R_f = 0.9-1.0). Instant thin layer chromatography (ITLC) was performed using silica gel-impregnated glass microfiber paper strips (ITLC-SG) from Agilent Technologies (Stockport, UK) and visualized using a Typhoon FLA 7000 scanner (GE Healthcare Life Sciences, UK). Citric acid used for the mobile phase was purchased from Sigma-Aldrich (Gillingham, Dorset, UK).

A)

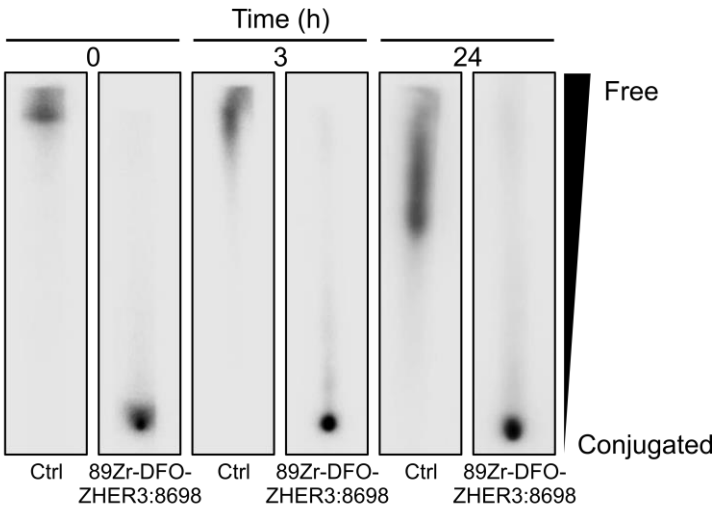

B)

0 h	3 h	24 h
100%	97.9 ± 0.4%	84.2 ± 0.9%

Fig. S8. Representative radio-ITLC of the ^{89}Zr-DFO-Z$_{HER3:8698}$ serum stability at 0, 3 and 24 h. (A) ^{89}Zr-oxalate was used as control. Radio-ITLC was run on silica-impregnated ITLC strips using 0.1 M citrate buffer (pH 5.0) as the mobile phase. ^{89}Zr-oxalate was used as control. The radiolabeled protein remains at the origin (R_f = 0.0-0.1) while un-bound radiometal migrates with the solvent front (R_f = 0.9-1.0). **(B)** The table indicates the % of radioactivity associated with the affibody molecule (R_f = 0.0-0.1) after 0, 3 and 24 h incubation.

	MCF-7		MDA-MB-468		MDA-MB-231		MCF-7 (Z$_{TAQ}$)	
Tissue	**%ID/g**	**T/organ**	**%ID/g**	**T/organ**	**%ID/g**	**T/organ**	**%ID/g**	**T/organ**
Blood	0.57 ± 0.09	4.75 ± 0.46	0.64 ± 0.19	2.18 ± 0.84	0.78 ± 0.02	0.71 ± 0.31	0.13 ± 0.02	1.30 ± 0.32
Heart	0.31 ± 0.07	8.69 ± 1.56	0.34 ± 0.07	3.94 ± 1.14	0.51 ± 0.13	1.11 ± 0.48	0.10 ± 0.01	1.65 ± 0.25
Lungs	1.10 ± 0.01	2.43 ± 0.29	1.31 ± 0.37	1.05 ± 0.34	1.63 ± 0.17	0.33 ± 0.11	0.18 ± 0.03	0.95 ± 0.35
Kidney	85.67 ± 8.2	0.03 ± 0.01	101.7 ± 25.6	0.01 ± 0.01	154.3 ± 14.9	0.01 ± 0.01	145.6 ± 12	0.01 ± 0.001
Spleen	0.36 ± 0.07	7.63 ± 0.81	0.44 ± 0.12	3.15 ± 1.21	0.37 ± 0.07	1.48 ± 0.48	0.21 ± 0.02	0.76 ± 0.14
Liver	2.29 ± 0.38	1.18 ± 0.13	2.20 ± 0.33	0.60 ± 0.13	3.23 ± 0.21	0.18 ± 0.08	0.69 ± 0.01	0.24 ± 0.06
Pancreas	0.44 ± 0.06	6.14 ± 0.70	0.36 ± 0.01	3.60 ± 0.45	0.60 ± 0.12	0.89 ± 0.21	0.10 ± 0.01	1.59 ± 0.26
Tumor (T)	2.67 ± 0.32	-	1.28 ± 0.13	-	0.55 ± 0.25	-	0.17 ± 0.04	-
Bone	0.48 ± 0.09	5.69 ± 1.56	0.45 ± 0.13	3.10 ± 1.13	0.46 ± 0.04	1.18 ± 0.41	0.18 ± 0.02	0.93 ± 0.18
S. I.	3.67 ± 1.16	0.80 ± 0.36	2.59 ± 0.32	0.50 ± 0.11	4.65 ± 0.50	0.12 ± 0.07	0.11 ± 0.01	1.55 ± 0.26
Muscle	0.14 ± 0.04	20.4 ± 4.93	0.11 ± 0.03	12.1 ± 2.04	0.20 ± 0.05	2.76 ± 0.75	0.06 ± 0.02	2.83 ± 0.18

Table S2. **Biodistribution results for ^{89Zr}-DFO-Z$_{HER3:8698}$ and ^{89}Zr-DFO-Z$_{TAQ}$ (3 µg, 7.2-8.1 MBq/mouse) at 3 h after injection.** The data are expressed as the mean values ± SD per xenograft model (*n* = 3 animals) per organ (S. I., small intestine).

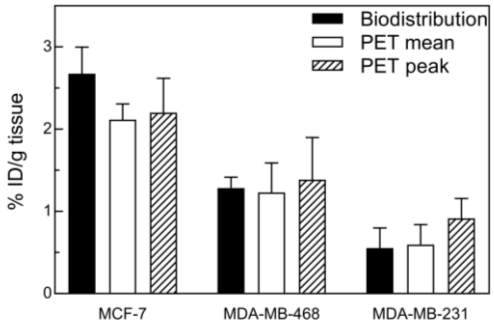

Fig. S9. *In vivo* ^{89}Zr-DFO-$Z_{HER3:8698}$ tumor uptake quantification by image analysis. MCF-7, MDA-MB-468, and MDA-MB-231 xenografts were injected with ^{89}Zr-DFO-$Z_{HER3:8698}$ (3 μg, 7.2-8.1 MBq/mouse) and subsequently underwent a PET/CT scan at 3 h after injection. The *ex vivo* biodistribution-determined %ID/g value was compared to the PET mean (mean %ID/g within the segmented tumor) and PET peak (mean %ID/g of the 500 hottest voxels within the segmented tumor) determined by image analysis. No statistically significant difference was observed in any of the xenograft models.

	MCF-7 (%ID/g)		MDA-MB-468 (%ID/g)	
Tissue	**3 h**	**24 h**	**3 h**	**24 h**
Blood	0.57 ± 0.09	0.18 ± 0.13	0.64 ± 0.19	0.38 ± 0.29
Heart	0.31 ± 0.07	0.26 ± 0.17	0.34 ± 0.07	0.21 ± 0.04
Lungs	1.10 ± 0.01	0.51 ± 0.13	1.31 ± 0.37	0.46 ± 0.03
Kidney	85.67 ± 8.2	83.04 ± 10.76	101.73 ± 25.6	74.65 ± 12.04
Spleen	0.36 ± 0.07	0.33 ± 0.16	0.44 ± 0.12	0.38 ± 0.13
Liver	2.29 ± 0.38	1.85 ± 0.40	2.20 ± 0.33	1.71 ± 0.42
Pancreas	0.44 ± 0.06	0.34 ± 0.30	0.36 ± 0.01	0.28 ± 0.12
Tumor	2.67 ± 0.32	1.38 ± 0.57	1.28 ± 0.13	1.08 ± 0.32
Bone	0.48 ± 0.09	1.56 ± 0.72	0.45 ± 0.13	1.37 ± 0.42
Small Intestine	3.67 ± 1.16	1.32 ± 0.18	2.59 ± 0.32	1.12 ± 0.19
Muscle	0.14 ± 0.04	0.09 ± 0.04	0.11 ± 0.03	0.11 ± 0.06

Table S3. Biodistribution results for ^{89}Zr-DFO-$Z_{HER3:8698}$ at 3 h and 24 h after injection in MCF-7 and MDA-MB-468 tumor-bearing mice. The data are expressed as the mean values ± SD per xenograft model per time point (n = 3 animals).

	MCF-7 (Tumor/organ)		MDA-MB-468 (Tumor/organ)	
Tissue	**3 h**	**24 h**	**3 h**	**24 h**
Blood	4.75 ± 0.46	9.58 ± 4.66	2.18 ± 0.84	3.51 ± 1.43
Heart	8.69 ± 1.56	5.81 ± 1.22	3.94 ± 1.14	5.19 ± 0.92
Lungs	2.43 ± 0.29	2.62 ± 0.46	1.05 ± 0.34	2.34 ± 0.68
Kidney	0.031 ± 0.01	0.02 ± 0.00	0.01 ± 0.01	0.01 ± 0.00
Spleen	7.63 ± 0.81	4.22 ± 0.36	3.15 ± 1.21	2.88 ± 0.54
Liver	1.18 ± 0.13	0.73 ± 0.15	0.60 ± 0.13	0.63 ± 0.05
Pancreas	6.14 ± 0.70	5.39 ± 2.82	3.60 ± 0.45	4.00 ± 0.85
Tumor	-	-	-	-
Bone	5.69 ± 1.56	1.12 ± 0.93	3.10 ± 1.13	0.81 ± 0.26
Small Intestine	0.80 ± 0.36	1.10 ± 0.63	0.50 ± 0.11	0.95 ± 0.16
Muscle	20.37 ± 4.93	14.86 ± 0.72	12.08 ± 2.04	11.10 ± 3.03

Table S4. **Tumor/organ ratios for ^{89}Zr-DFO-Z$_{HER3:8698}$ at 3 h and 24 h after injection in MCF-7 and MDA-MB-468 tumor-bearing mice.** The data are expressed as the mean values ± SD per xenograft model per time point (*n* = 3 animals).

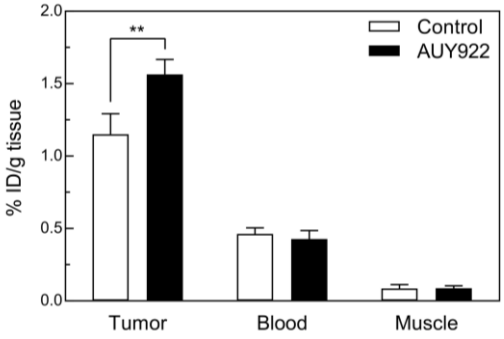

Fig. S10. *Ex vivo* biodistribution of ^{89}Zr-DFO-Z$_{HER3:8698}$ following AUY922 treatment in MCF-7 xenografts. The mice were randomized to control or treatment groups, with the treatment group receiving 40 mg/kg of AUY922 every second day for a period of 14 days. *Ex vivo* biodistribution was performed at 3 h after injection of the radioconjugate on day 14. Data are expressed as the mean values ± SD per control (*n* = 4 animals) and AUY922 treatment group *(n* = 6 animals). ***P* = 0.0036.

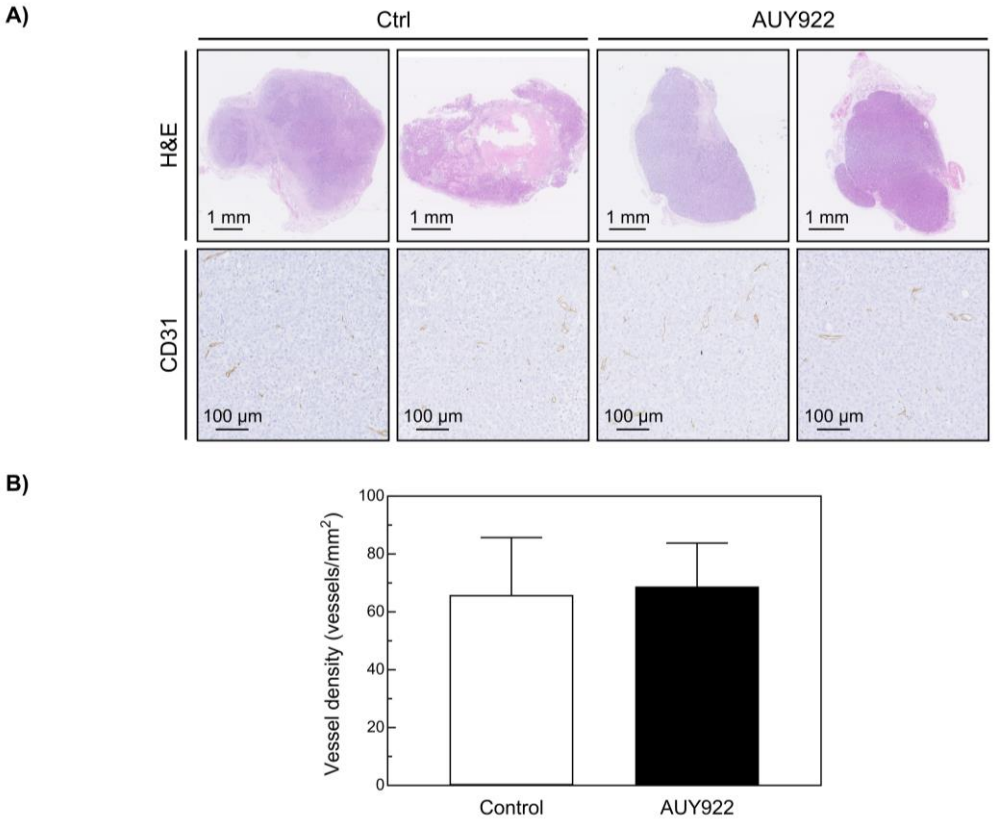

Fig. S11. Microvessel density analysis in response to AUY922 treatment in MCF-7 xenografts. (A) Representative histopathological micrographs of control and AUY922-treated MCF-7 xenografts. Tumor sections were stained with hematoxylin and eosin (H&E), and CD31. **(B)** Microvessel density quantification data expressed as the mean values ± SD per control (*n* = 6 animals) and AUY922 treatment group (*n* = 7 animals), with no statistically significant difference observed between groups.

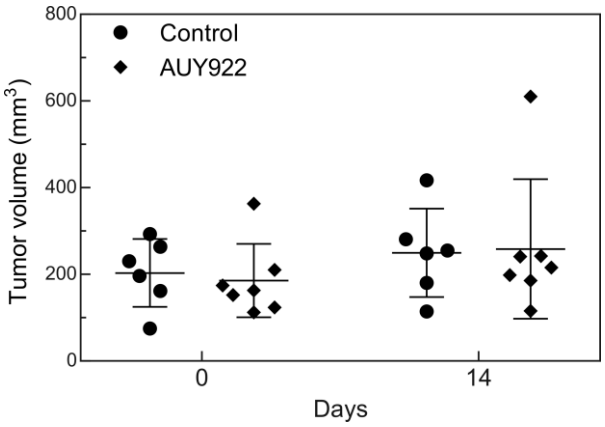

Fig. S12. Tumor volume estimation in response to AUY922 treatment in MCF-7 xenografts. MCF-7 xenografts were treated with either saline (control) or 40 mg/kg of AUY922. Tumor volumes were estimated by manually segmenting each tumor on the CT images acquired before treatment initiation (day 0) and after the last dose was administered (day 14). The data are expressed as the mean values ± SD per control (*n* = 6 animals) and AUY922 treatment group (*n* = 7 animals).

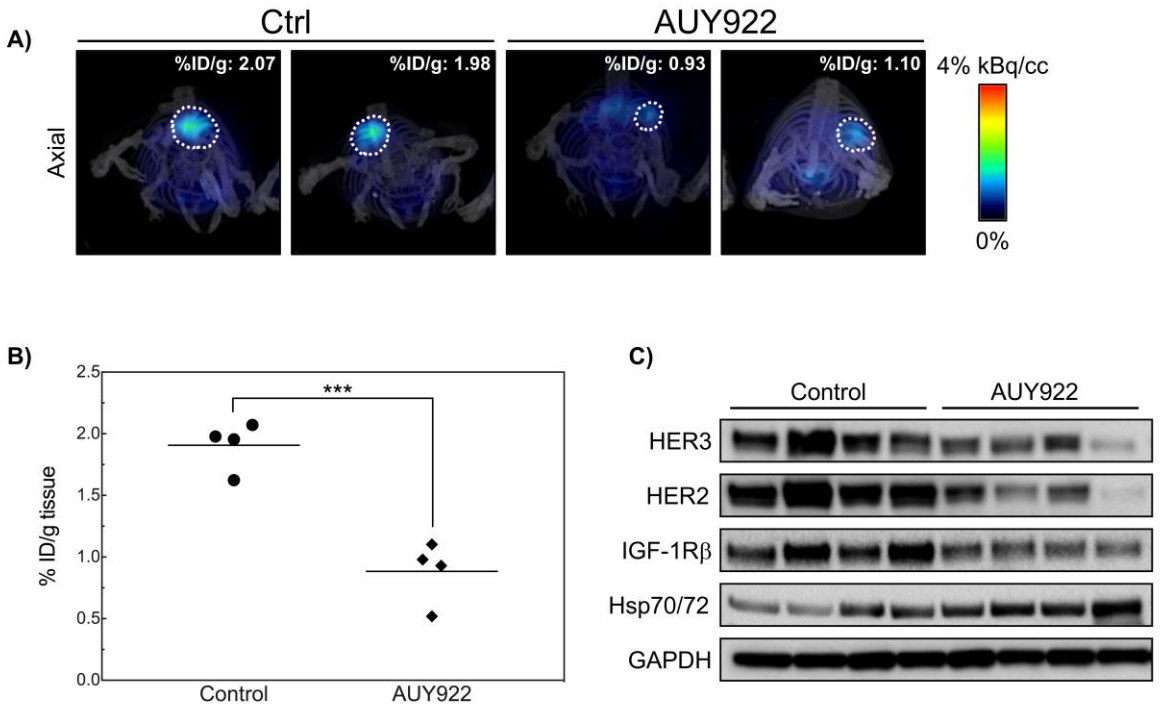

Fig. S13. AUY922 treatment response monitoring in BT-474 xenografts by ^{89}Zr-DFO-Z$_{HER3:8698}$ PET/CT imaging. BT-474 xenografts were randomized into two groups: control and treatment. The treatment group received 6 doses of 50 mg/kg of AUY922 i.p. during a period of two weeks. **(A)** Representative axial fused PET/CT images of mice bearing BT-474 tumors. Each mouse received 7.2-8.1 MBq of ^{89}Zr-DFO-Z$_{HER3:8698}$ via tail vein injection, with image acquisition taking place at 3 h after injection. The mice were imaged following administration of the last treatment dose (day 14). **(B)** Scatter plot of the %ID/g tumor tissue for both control (*n* = 4) and AUY922-treated mice *(n* = 4). The horizontal lines indicate the mean for each group. ****P* = 0.0009. **(C)** HER receptors and IGF-1Rβ were monitored by Western blot using whole tissue lysates from all control and AUY922-treated mice. Hsp70/72 expression was used as a surrogate for AUY922 treatment efficacy, and GAPDH as a loading control.

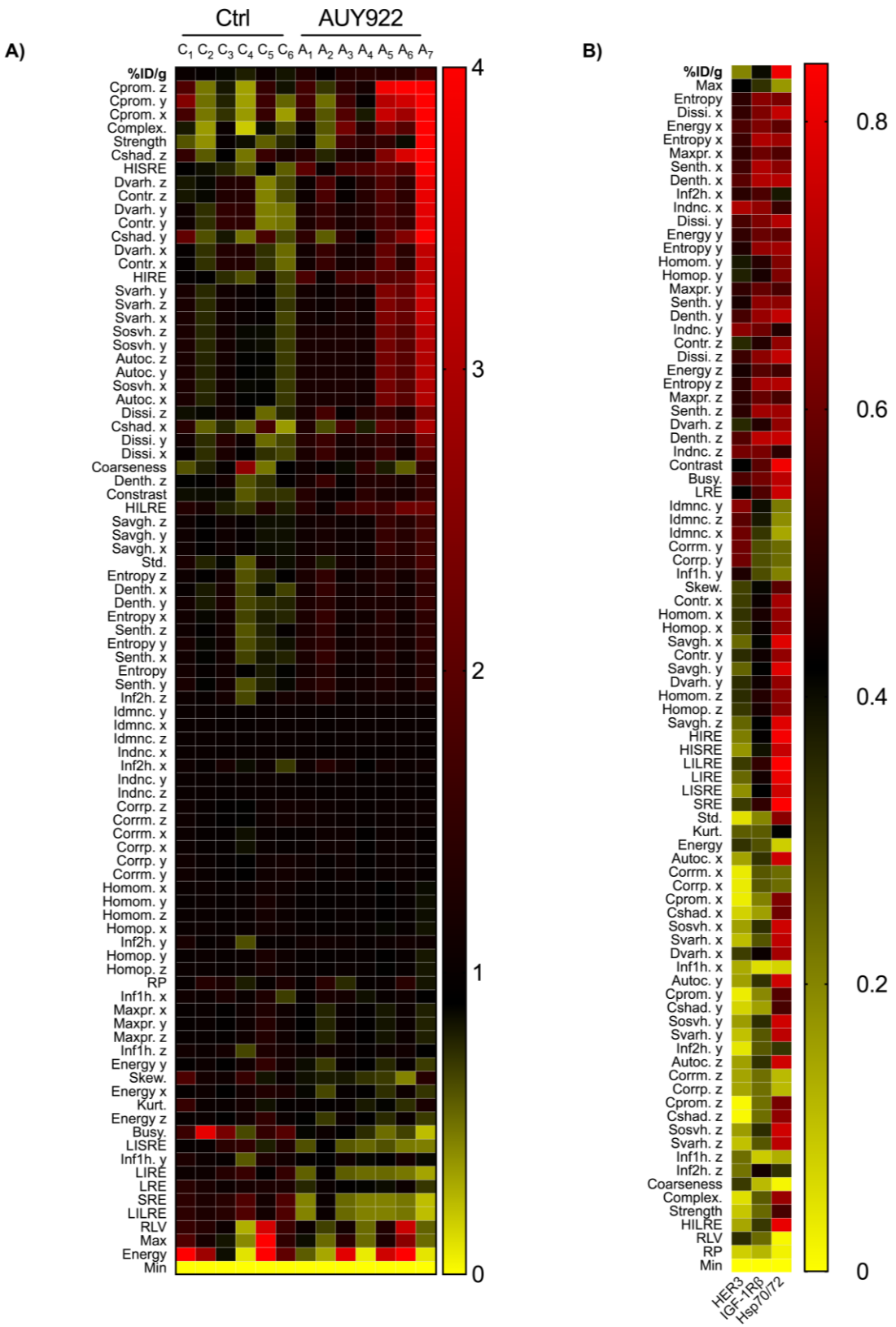

Fig. S14. Texture analysis of ^{89}Zr-DFO-Z$_{HER3:8698}$ PET imaging data following AUY922 treatment in MCF-7 xenografts. (A) Texture analysis heat map comprising the ratios of post/pre-treatment for all 89 extracted texture parameters per mouse (Control $C_{1\text{-}6}$, and AUY922 $A_{1\text{-}7}$). **(B)** Correlation heat map comprising the correlations established between all extracted texture parameters in (A) and HER3, IGF-1Rβ, and Hsp70/72 expression levels represented in Fig. 6A. 41.6% of the 89 parameters have a ≥0.35 correlation with HER3 expression, 58.4% of the 89 parameters have a ≥0.35 correlation with IGF-1Rβ, and 77.5% of the parameters have a ≥0.35 correlation with Hsp70/72 expression. 34% of the parameters have a ≥0.35 correlation simultaneously between HER3, IGF-1Rβ and Hsp70/72.

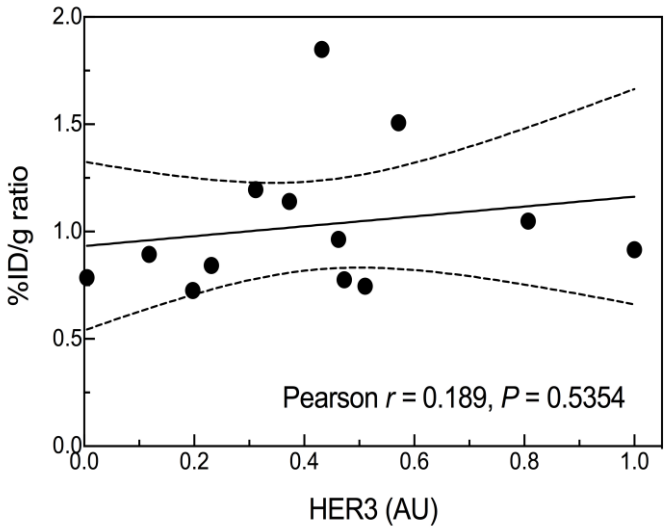

Fig. S15. Correlation between %ID/g ratios obtained from ^{89}Zr-DFO-Z$_{HER3:8698}$ PET images and HER3 protein expression per control and AUY922-treated MCF-7 xenografts. The dashed lines represent the ninety-five percent confidence levels.

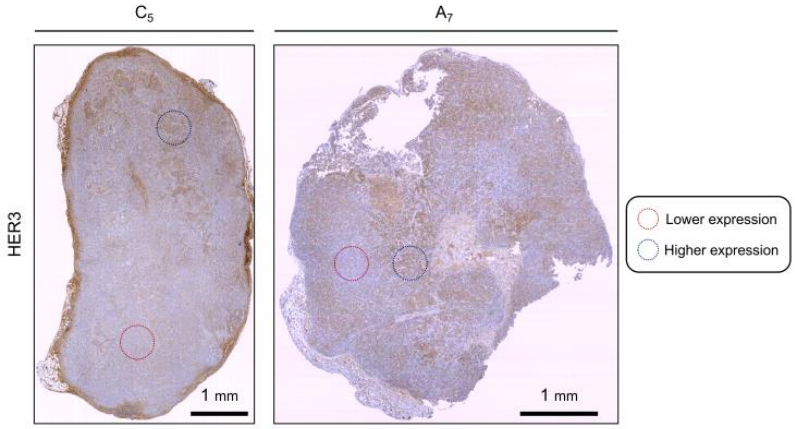

Fig. S16. HER3 intra-tumoral heterogeneity highlighted by histopathological analysis of control and AUY922-treated MCF-7 xenografts. Tumor sections were stained with hematoxylin and eosin (H&E), and HER3. The blue and red circles highlight areas of more and less prominent HER3 staining, respectively.

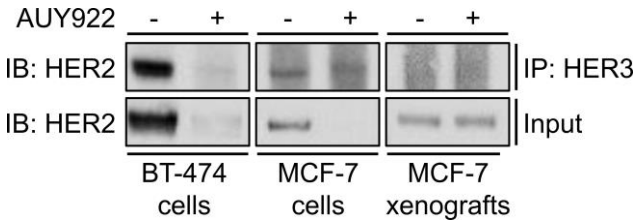

Fig. S17. HER2-HER3 interaction in BT-474 and MCF-7 cells following AUY922 treatment. T-474 and MCF-7 cells were treated with 32 nM of AUY922 for 48 h. Equal amounts of whole cell lysates were immunoprecipitated with a mouse anti-HER3 antibody followed by WB analysis of the HER2 receptor. Ten percent of the input lysates were used as loading controls.

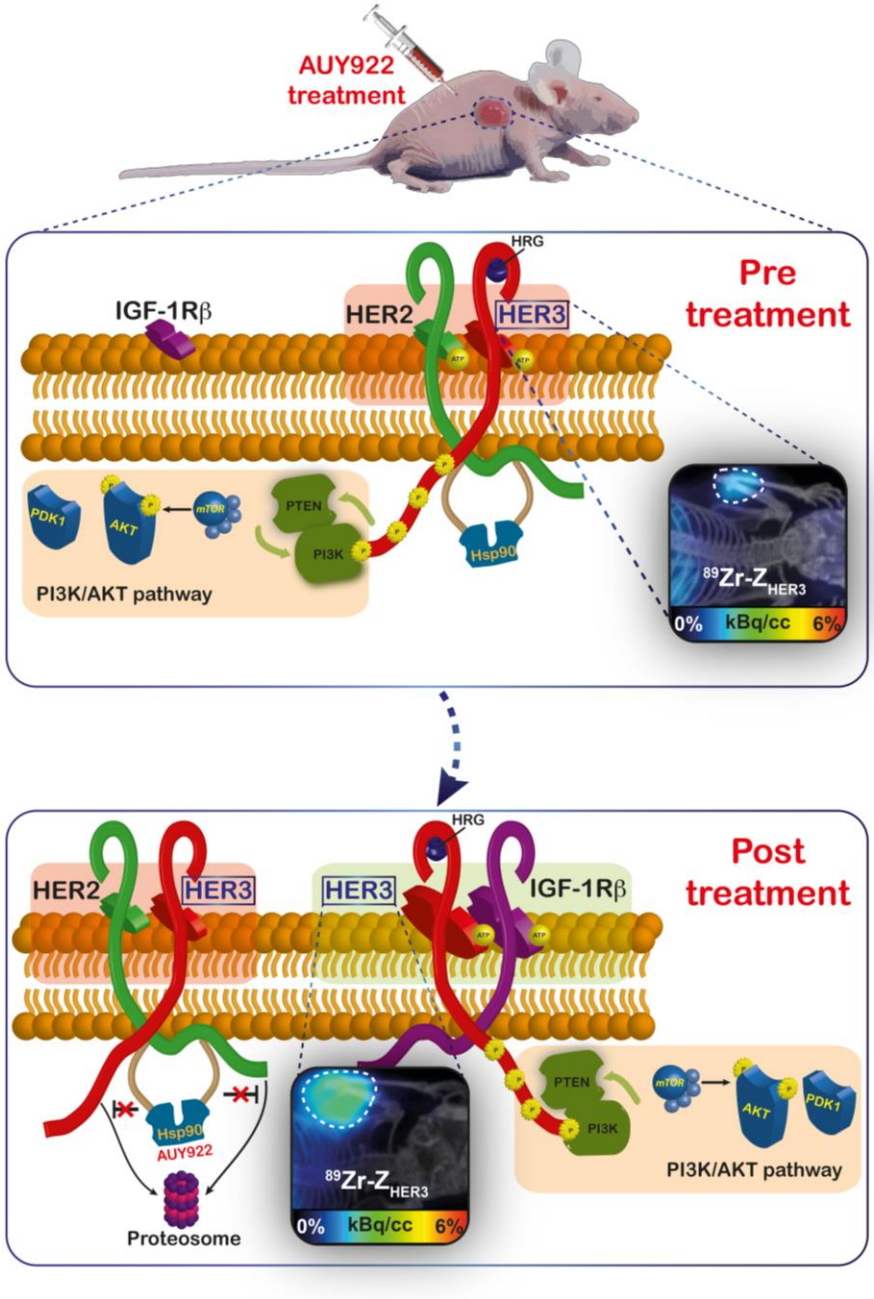

Fig. S18. Scheme illustrating the proposed effect of AUY922-induced Hsp90 inhibition in MCF-7 breast cancer xenografts. MCF-7 cells express low levels of HER2, conventionally heterodimerized with the HER3 receptor. Following HRG ligand binding, the HER3 receptor becomes active and leads to the activation of the PI3K/AKT/mTOR pathway. Hsp90 is a chaperone protein which confers conformational stability to the HER2 receptor, allowing HER2-HER3 mediated pathway activation to take place. HER3 expression can be monitored *in vivo* using ^{89}Zr-Z$_{HER3}$ PET imaging probe. In response to treatment with the Hsp90 inhibitor AUY922, most likely HER2-HER3 dimers get internalized, subsequently undergoing a proteasome-mediated degradation that results in a transient deactivation of the PI3K/AKT/mTOR signalling. Constant exposure to AUY922 promotes both an increase in HER3 and IGF-1Rβ expression and their heterodimerization. As a consequence the PI3K/AKT/mTOR pathway is re-activated, resulting in the establishment of an AUY922 resistance mechanism in a low-HER2 background. The increased HER3 level is indicated by ^{89}Zr-Z$_{HER3}$ uptake in the treated tumour.

Gene A	Gene B	P-value	Log Odds Ratio	Association *HER3:IGF1R*
HER3	*IGF1R*	0.020	0.921	Tendency towards co-occurrence (significant)

Table S5. *HER3* and *IGF1R* co-occurrence in breast invasive carcinoma samples. The TCGA Provisional dataset comprising 1105 breast invasive carcinoma samples was queried for *HER3* and *IGF1R* mRNA expression in all samples. Mutual exclusivity analysis revealed a significant co-occurrence tendency between the indicated genes.

	Total cases	Cases deceased	Median months survival	Logrank Test P-value
Alterations in *HER3*, *IGF1R*	126	22	95.63	0.0332
No alterations	967	130	129.6	

Table S6. *HER3* and *IGF1R* alterations lead to a shorter overall survival in breast invasive carcinoma samples. The TCGA Provisional dataset comprising 1105 breast invasive carcinoma samples was queried for *HER3* and *IGF1R* mRNA expression in all samples. Survival analysis revealed shorter overall survival rates when alterations are found in the indicated genes.

	Total cases	Cases relapsed	Median months disease free	Logrank Test P-value
Alterations in *HER3*, *IGF1R*	113	17	138.07	0.0309
No alterations	888	95	214.72	

Table S7. *HER3* and *IGF1R* alterations lead to a shorter disease free survival in breast invasive carcinoma samples. The TCGA Provisional dataset comprising 1105 breast invasive carcinoma samples was queried for *HER3* and *IGF1R* mRNA expression in all samples. Survival analysis revealed shorter disease free survival rates when alterations are found in the indicated genes.

Gene A	Gene B	P-value	Log Odds Ratio	Association *HER3:IGF1R*
HER3	*IGF1R*	0.314	1.262	Tendency towards co-occurrence

Table S8. *HER3* and *IGF1R* co-occurrence in HER2 up-regulated breast invasive carcinoma samples. The TCGA Provisional dataset comprising 1105 breast invasive carcinoma samples was queried for *HER2* mRNA expression in all samples. The *HER2* up-regulated samples were then queried for *HER3* and *IGF1R* mRNA expression. Mutual exclusivity analysis revealed no statistically significant co-occurrence tendency between the indicated genes when *HER2* is up-regulated.

SM References

1. Da Pieve C, Allott L, Martins CD, Vardon A, Ciobota DM, Kramer-Marek G, et al. Efficient [18F]AlF Radiolabeling of ZHER3:8698 Affibody Molecule for Imaging of HER3 Positive Tumors. Bioconjugate Chemistry. 2016.
2. Vosjan MJWD, Perk LR, Visser GWM, Budde M, Jurek P, Kiefer GE, et al. Conjugation and radiolabeling of monoclonal antibodies with zirconium-89 for PET imaging using the bifunctional chelate p-isothiocyanatobenzyl-desferrioxamine. Nat Protoc. 2010;5:739-43.
3. Chicklore S, Goh V, Siddique M, Roy A, Marsden PK, Cook GJ. Quantifying tumour heterogeneity in 18F-FDG PET/CT imaging by texture analysis. European Journal of Nuclear Medicine and Molecular Imaging. 2013;40:133-40.